Journal of Alloys and Compounds 858 (2021) 158372

Contents lists available at ScienceDirect

Journal of Alloys and Compounds

journal homepage: www.elsevier.com/locate/jalcom

Preparation and properties of novel activated carbon doped with aluminum oxide and silver for water treatment

Rashad Al-Gaashani[a,b,*], Dema Almasri[a], Basem Shomar[c], Viktor Kochkodan[a]

[a] Qatar Environment and Energy Research Institute (QEERI), Hamad Bin Khalifa University (HBKU), Qatar Foundation, 34110 Doha, Qatar
[b] Physics Department, Faculty of Education, Thamar University, Dhamar, Republic of Yemen
[c] Environmental Science Center (ESC), Qatar University, 2713 Doha, Qatar

ARTICLE INFO

Article history:
Received 15 September 2020
Received in revised form 27 November 2020
Accepted 14 December 2020
Available online 17 December 2020

Keywords:
Activated carbon doped with Al_2O_3 and silver
Adsorption
Arsenic
Molybdenum
Antibacterial properties

ABSTRACT

Novel activated carbon (AC) composite materials, namely AC doped with aluminum oxide (Al_2O_3) and AC doped with Al_2O_3 and silver (Ag) nanoparticles, have been prepared via a one-step thermal decomposition method. The developed composite materials were used to study the adsorptive removal of molybdenum (Mo) and arsenic (As) from contaminated water. Several techniques, including X-Ray diffraction (XRD), transmission electron microscopy (TEM), scanning electron spectroscopy (SEM), energy dispersive X-Ray spectroscopy (EDS), and thermal gravimetric analysis (TGA), were used to characterize the synthesized materials. TGA results show that the material is very stable and decay starts only above 450 °C. The effects of pH on the adsorptive removal of As and Mo on AC-Al_2O_3 have also been studied. The prepared AC-Al_2O_3 material showed 94% removal of total As at pH of 6% and 97% removal of Mo at pH 2. The pollutants removal is due to electrostatic attraction and ligand exchange adsorption mechanisms. It was also found that the novel AC-Al_2O_3-Ag composite materials exhibit notable antibacterial properties towards both Gram-negative (*Escherichia coli*) and Gram-positive (*Bacillus subtilis*) bacteria.

1. Introduction

Due to their large surface area and microporous nature, activated carbon (AC) and modified activated carbons are used in multiple applications such as water treatment [1–4], gas/air purification [5], metal extraction [6], medical applications [7,8], catalysis [9–11], bio- and environmental applications [12,13], and energy storage applications [14,15]. AC is effective in adsorbing a wide range of organic compounds [16] and bacterial nutrients [17]. However, some studies have shown that AC used to treat drinking water can be heavily occupied by microbes, while other studies have revealed that bacteria attached to AC can be resistant to chlorination [18–21]. Although AC is among the best adsorbents available in the market, there are still several problems and challenges related to its sorption capacity and low removal rates of heavy metals and bacteria. For example, it was reported that AC has a low efficiency in removing arsenic (As) from drinking water [22]. However, AC modified with iron materials were shown to considerably enhance the ability of iron-activated carbon composites for As removal when compared to pure AC filters [22,23]. Flocculated aluminum hydroxide produced from aluminum sulfate, aluminum oxide and iron oxide have been reported to be effective media for the removal of heavy metals, specifically, As [24–26].

Both As as well as molybdenum (Mo) are naturally occurring elements found in soils, sediments, and groundwater. However, their increasing presence due to anthropogenic activities is of concern due to detrimental effects on groundwater and surface waters. While As adsorption from water is well studied [27], very little information is available on Mo removal [28].

The study of Mondal and Garg [29] utilized AC from waste materials to be used for As adsorption and found the maximal removal to be at pH 1. Recent studies showed progress on the removal of arsenic from contaminated water. Both iron-modified and manganese-modified AC were studied as alternative sorbents for the removal of As(V) from aqueous solutions [30]. AC prepared from the natural products of oat hulls was found to be effective for the adsorption of As(V) [31]. Granular AC was also found to be effective towards the adsorption of Mo from aqueous solutions [3,32].

Although nowadays, different adsorbents, including AC, zeolite, kaolinite, bentonite, montmorillonite, sepiolite and halloysite clay are widely used for water treatment applications, there remains a

* Corresponding author at: Qatar Environment and Energy Research Institute (QEERI), Hamad Bin Khalifa University (HBKU), Qatar Foundation, 34110 Doha, Qatar.
E-mail address: ralgaashani@hbku.edu.qa (R. Al-Gaashani).

https://doi.org/10.1016/j.jallcom.2020.158372
0925-8388/

Table 1
Some physicochemical properties of activated carbon (AC) and doped activated carbon.

Physicochemical properties	AC	AC + 10 wt% Al_2O_3	AC + 10 wt% Al_2O_3 + 5 wt% Ag
Partials size[a]	50–200 (μm)	50–200 (μm) of AC doped with Al_2O_3 nanoparticles	50–200 (μm) of AC doped with Al_2O_3 and Ag nanoparticles
Surface area (S_{BET})[b](m^2/g)	1271.33	1162.77	1209.497
Total pore volume (cm^3/g)[c]	0.54	0.49	0.46
C (atomic percentage) (at%)[d]	97.35	93.21	67.14[e]
O (atomic percentage) (at%)[d]	2.34	4.24	23.22[e]
pH_{pzc}[f]	2.73	6.62	Not measured

[a] Partials size was determined by SEM and TEM.
[b] BET surface area (S_{BET}) was determined by using N_2 adsorption-desorption analysis at 77 K using a Micromeritics ASAP-2020 surface analyzer (USA).
[c] Total pore volume was calculated at p/p° = 0.995.
[d] Atomic percentage was determined by energy dispersive X-ray spectroscopy (EDS).
[e] Atomic percentage was determined by X-ray photoelectron spectroscopy (XPS). (The XPS results are not shown here).
[f] pH_{pzc}: pH at point of zero charge was determined by a Malvern Zetasizer Ultra equipment.

need to develop even more efficient and inexpensive sorbents and filters, especially for use in contaminated areas. Many attempts have been done worldwide to solve these challenges by using modified AC-based composite materials [33–37]. It was shown that AC doped/impregnated with silver can be efficiently used for bacteria removal from water [35,38–41]. Additionally, an AC/Fe-Al_2O_3 composite has been used as catalyst for hydrogen production [42], and AC-supported alumina (Al_2O_3) has been employed in the oxidation of phenol using a modified carbon electrode [43].

Alumina exhibits a unique ion exchange selectivity and presents both anion and cation exchange properties due to its acidic and basic properties [44]. So far, studies on the preparation and use of AC doped with Al_2O_3 and silver (Ag) are almost absent, and AC-Al_2O_3-Ag filters are not available in the markets. In this study, we report a novel, simple and robust approach to synthesize AC impregnated with silver and Al_2O_3 by using a one-step thermal decomposition method. The developed materials were tested for adsorptive removal of As and Mo from water. The antibacterial properties of AC and modified AC were also evaluated against *Escherichia coli* (*E. coli*) and *Bacillus subtilis* (*B. subtilis*) bacteria.

2. Experiments

2.1. Materials

Materials and chemicals that were used in this study were purchased from commercial suppliers of analytical grades. Activated carbon pieces with millimeter sizes, aluminum nitrate nonahydrate (Al $(NO_3)_3{\cdot}9H_2O$, purity 99.997%), silver nitrate ($AgNO_3$, 99%) and sodium hydroxide (NaOH, purity 99.99%) were all purchased from Sigma Aldrich (USA). Standard solutions of arsenic (As) (1000 mg/L) and molybdenum (Mo) (1000 mg/L) were purchased from ROMIL Pure Chemistry. Sodium nitrate and the standard solution of fluoride (1000 mg/L) were purchased from Merck. Aqueous solutions were prepared using deionized water (DIW) of 18.2 MΩ/cm. Some physicochemical properties of AC and doped AC samples are shown in Table 1.

2.2. Preparation of AC doped with aluminum oxide and silver

First, the AC pieces were ground to powder down to 50–200 μm size particles (BET surface area of 1271 m^2/g, see Table 1) using a ball mill method. Thereafter, composite materials consisting of 90 wt% AC/10 wt% Al_2O_3 and 85 wt% AC/10 wt% Al_2O_3/5 wt% silver were synthesized by quick thermal decomposition of aluminum nitrate nonahydrate and silver nitrate in a muffle furnace (Thermo Scientific Thermolyne 5.8 L A1 Bench top Muffle Furnace, 240 V) under air atmosphere at 450 °C for 60 min. In a typical experiment, 2 g of aluminum nitrate nonahydrate, 200 mg of NaOH, 1 g of silver nitrate and 20 g of AC powder were mixed in 100 mL of deionized water. The mixture was stirred for 20 min, followed by sonication for 10 min in an ultrasonic bath. The saturated AC was placed in an alumina crucible and was heated at 450 °C for 60 min. After the furnace was switched off, the AC doped with aluminum oxide and silver was cooled down to room temperature and taken out of the furnace. The AC composite material was then washed with deionized water for several times. Finally, the washed samples were dried in an oven at 95 °C for 24 h in air. Fig. 1 illustrates a diagram of experimental steps to prepare the AC-Al_2O_3-Ag composites.

2.3. Samples characterization

Several advanced techniques were used to characterize the prepared samples. The structural study of the materials was characterized using X-ray diffraction (XRD) patterns from a Bruker D8 Advance X-Ray diffractometer with Cu-Kα radiation source

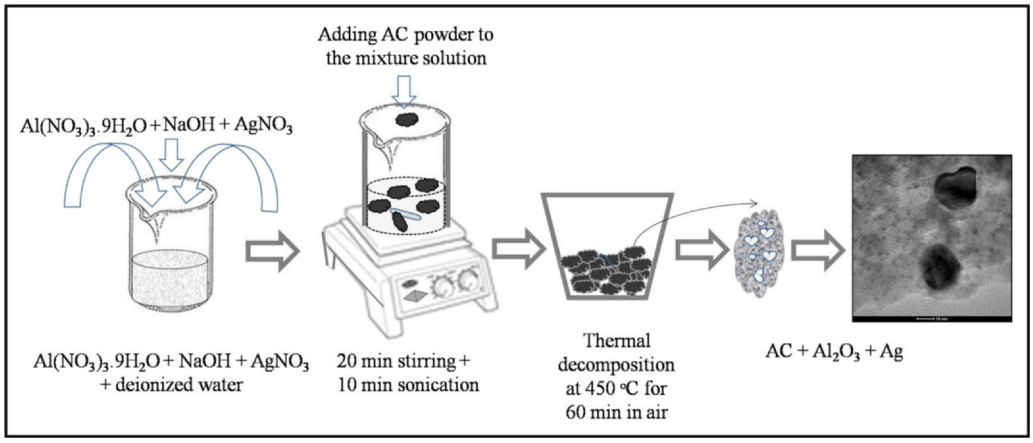

Fig. 1. A diagram shows experimental steps to prepare AC-Al_2O_3-Ag composites.

(λ = 0.15418 nm) ranging from 10° to 80°. High resolution transmission electron microscopy (HRTEM) (FEI Talos 200X) and scanning electron microscopy (SEM) (Quanta 650) were used to study the morphology of the prepared samples. Energy-dispersive X-ray spectroscopy (EDS) was used for elemental analysis. TGA was used to study the thermal stability using a Perkin-Elmer thermos-gravimetric system. A temperature range of 30–1000 °C at a heating rate of 10 °C/min under oxygen flow was used. Zeta potential measurements were done on a Malvern Zetasizer Ultra equipment. The BET surface area and total pore volume of the activated carbon and doped activated carbon samples were measured using N_2 adsorption-desorption analysis at 77 K using a micromeritics ASAP-2020 surface analyzer (USA). Before BET measuring, the samples were degassed at 200 °C for 8 h.

2.4. Batch adsorption experiments

In a typical adsorption experiment, 2.5 g/L of AC powder or AC doped with aluminum oxide (AC-Al_2O_3) were added to a solution with a known contaminant concentration. For the single and multi-element experiments, the pH was adjusted to 7.0 ± 0.2. The pH of the solution was adjusted with 0.1–1 M HCl or NaOH. The reactors were shaken at 25 °C at a rate of 350 rpm for 24 h (to ensure equilibrium adsorption was met). The effect of competition on Mo removal from water was investigated by adding common coexisting ions that may be found in groundwater (arsenic, fluoride, and nitrate) to the Mo solution. Sample aliquots were taken from the suspensions and filtered through a 0.45 µm filter for cation and anion analysis. The effect of solution pH on the adsorption of contaminants was studied by adjusting the initial pH from 2 to 8 after the addition of adsorbents.

Arsenic, molybdenum, and aluminum were analyzed using an inductively coupled plasma-mass spectrometry (ICP-MS) (Bruker aurora M90). Fluoride and nitrate ions were analyzed using an ion chromatography (IC, Dionex).

The percent removal at a specific time t of pollutants was calculated based on the following equation:

$$\%removal = \frac{(C_0 - C_t)}{C_0} \times 100\% \quad (1)$$

Here, C_0 (mg/L), and C_t (mg/L) denote the initial and equilibrium pollutants concentrations, respectively, V (L) is the volume of the solution, and W (g) is the mass of the adsorbent used.

2.5. Testing of the antimicrobial properties of the synthesized material

The antimicrobial activity of the synthesized materials against *Escherichia coli* (*E. coli*) and *Bacillus subtilis* (*B. subtilis*) bacteria was tested using agar cup double-diffusion methods [45]. The microorganisms were cultured overnight at 37 °C in nutrient agar. The cell concentrations of bacterial inoculants were 120–230 colony-forming unit (CFU)/mL. The carbon-based materials were delivered to the Petri dishes, and the Petri dishes were incubated at 37 °C for 24 h. After incubation, the zones of inhibition were evaluated by measuring the diameter of the zone formed around the materials. The presence of the zone of microbial growth inhibition around the carbon-based material indicates its bactericidal effect. This effect was expressed in terms of average diameter of the inhibition zone.

3. Results and discussion

3.1. Structural studies of the prepared samples

Fig. 2 shows XRD patterns of AC before doping (a), AC after doping with 10 wt% Al_2O_3 (b) and AC doped with 10 wt% Al_2O_3 and 5 wt% Ag (c). Fig. 2(a) depicts the amorphous phase of AC before doping. AC doped with 10 wt% Al_2O_3 has also amorphous phase as shown in Fig. 2(b). However, AC doped with 10% Al_2O_3 and 5 wt% Ag has two phases: an amorphous phase of AC doped Al_2O_3 and crystalline phase of Ag as shown in Fig. 2(c). The diffraction peaks observed at Bragg angle (2θ) of 38.11°, 44.30°, 64.45° and 77.41° correspond to, respectively, (111), (200), (220) and (311) planes of the cubic structure of Ag (ICDD card No. 01-087-0717 with a lattice constant equals to a: 4.0857 Å, volume: 68.20 $Å^3$ and space group *Fm*-3*m*) (Fig. 2c).

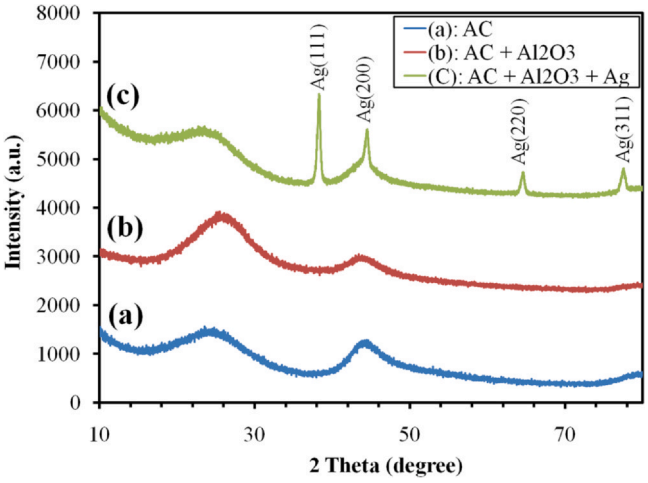

Fig. 2. XRD patterns of (a) AC, (b) AC + Al_2O_3 and (c) AC-Al_2O_3-Ag.

Fig. 3 shows surface SEM images of AC (a and b) and AC doped with 10 wt% Al_2O_3 (c and d) while cross section SEM images of AC doped with 10 wt% Al_2O_3 were shown in Fig. 3(e and f). The AC surface before modification is free of white particles (namely, Al_2O_3 nanoparticles) as shown in Fig. 3(a and b). However, after modification of AC using Al_2O_3, the white nanoparticles were regularly grew and distributed over the surface and cross section of AC, as shown in Fig. 3(c–f). After reacting aluminum nitrate with sodium hydroxide in deionized water, aluminum hydroxide was produced as shown in Eq. (2). The formed aluminum hydroxide was absorbed by AC particles during stirring.

$$Al(NO_3)_3 + 3NaOH \rightarrow Al(OH)_3 + 3NaNO_3 \quad (2)$$

During thermal decomposition of aluminum nitrate at 450 °C, aluminum oxide grew in every part of the AC particles, as shown in Figs. 3(c–f) and 5 (Al). Thermal decomposition of aluminum nitrate took place between about 150–200 °C as follows:

$$2Al(NO_3)_3 \overset{450°C}{\rightarrow} Al_2O_3 + 6NO_2 + 3/2O_2 \quad (3)$$

Figs. 4 and 5 illustrate EDS analysis of AC before and after doping with 10 wt% Al_2O_3, respectively. The elemental and mapping analysis by EDS of AC before doping show that C and O were the main elements, as shown in Fig. 4. However, EDS mapping (Fig. 5) shows three main elements (C, O and Al) after AC doping with 10 wt% Al_2O_3. Fig. 5 (Al) shows a uniform distribution of the Al element in AC particle.

Fig. 6 illustrates TEM images of AC doped with Al_2O_3 and Ag prepared by one-step thermal decomposition at 450 °C of aluminum nitrate nonahydrate and silver nitrate absorbed by AC. The black crystal particles represent silver nanoparticles while white-gray areas represent amorphous phases of AC doped with Al_2O_3. Silver nanoparticles have three different morphologies: quantum dots (less than 4 nm), heart morphology and apple morphology as shown in Fig. 6(d). The nano-heart shaped structure has about 25 nm length and 26 nm width (Fig. 6c). Similarity, nano-apple shaped structure has about 20 nm length and 25 nm width (Fig. 6e). Fig. 7 provides

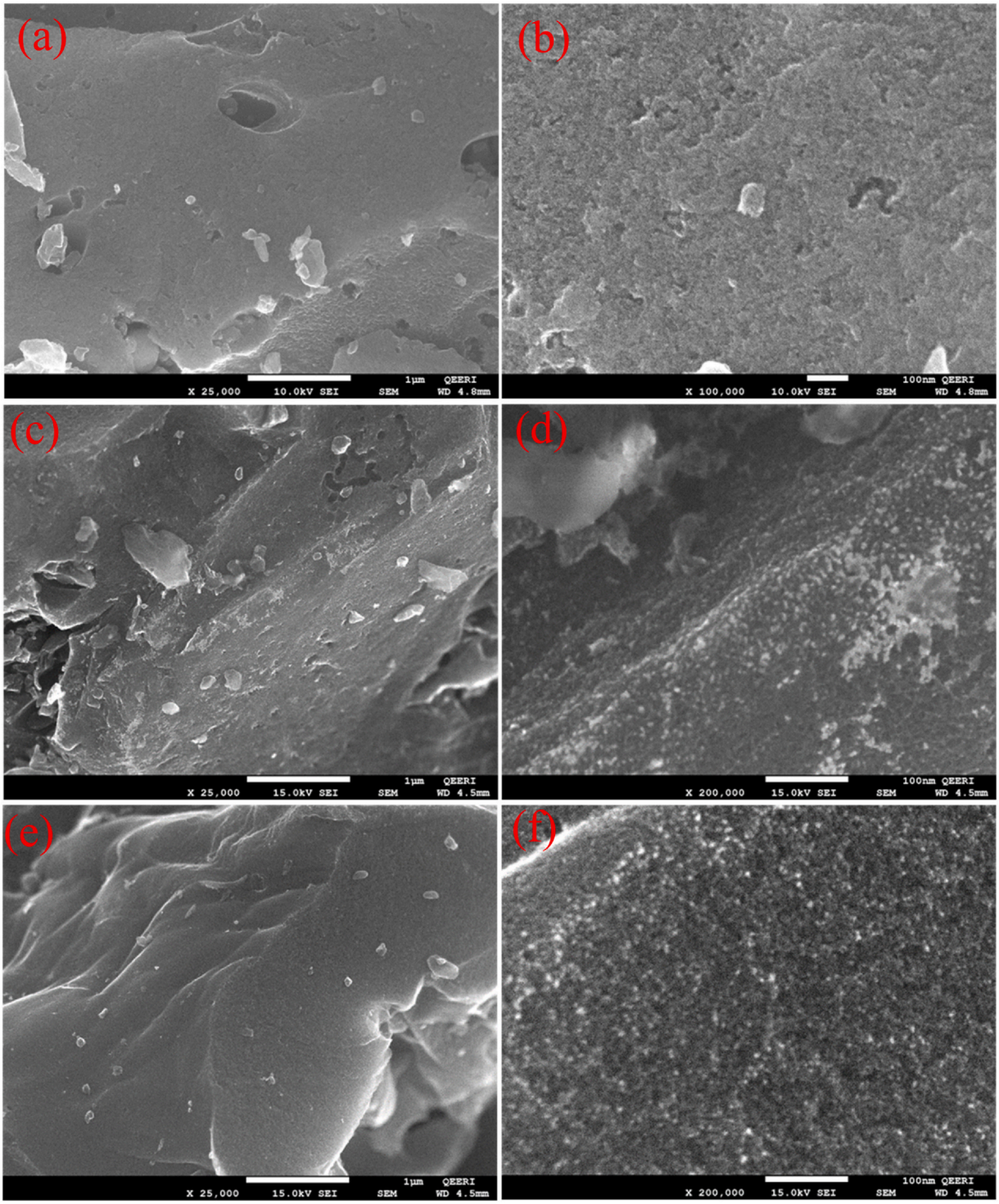

Fig. 3. SEM images of AC as it is (a and b) and AC doped with 10 wt% Al_2O_3 (c–f).

EDS analyses of AC doped with 10 wt% Al_2O_3 and 5 wt% Ag. The elemental and mapping analysis by EDS of AC show that C, Ag, Al and O are the main elements as shown in Fig. 7.

Fig. 8 depicts the TGA analysis of AC (a) and AC doped with 10 wt% Al_2O_3 (b). These results reveal that composite materials are very stable at ambient temperatures and decay starts only above 450 °C. The rest of the materials after burning the activated carbon represent about 1 wt% (a) and 11 wt% (b) which includes 10 wt% Al_2O_3.

Table 1 shows that there is no appreciable effect on porous structure or surface area of AC after thermal decomposition of nitrates.

3.2. Adsorption properties

AC and AC-Al_2O_3 were tested for their adsorption removal efficiency in a multi-element solution consisting of coexisting ions commonly found in natural water, which include Mo, As, F, and NO_3 at a pH 7. From Fig. 9, it can be seen that negligible amounts of all

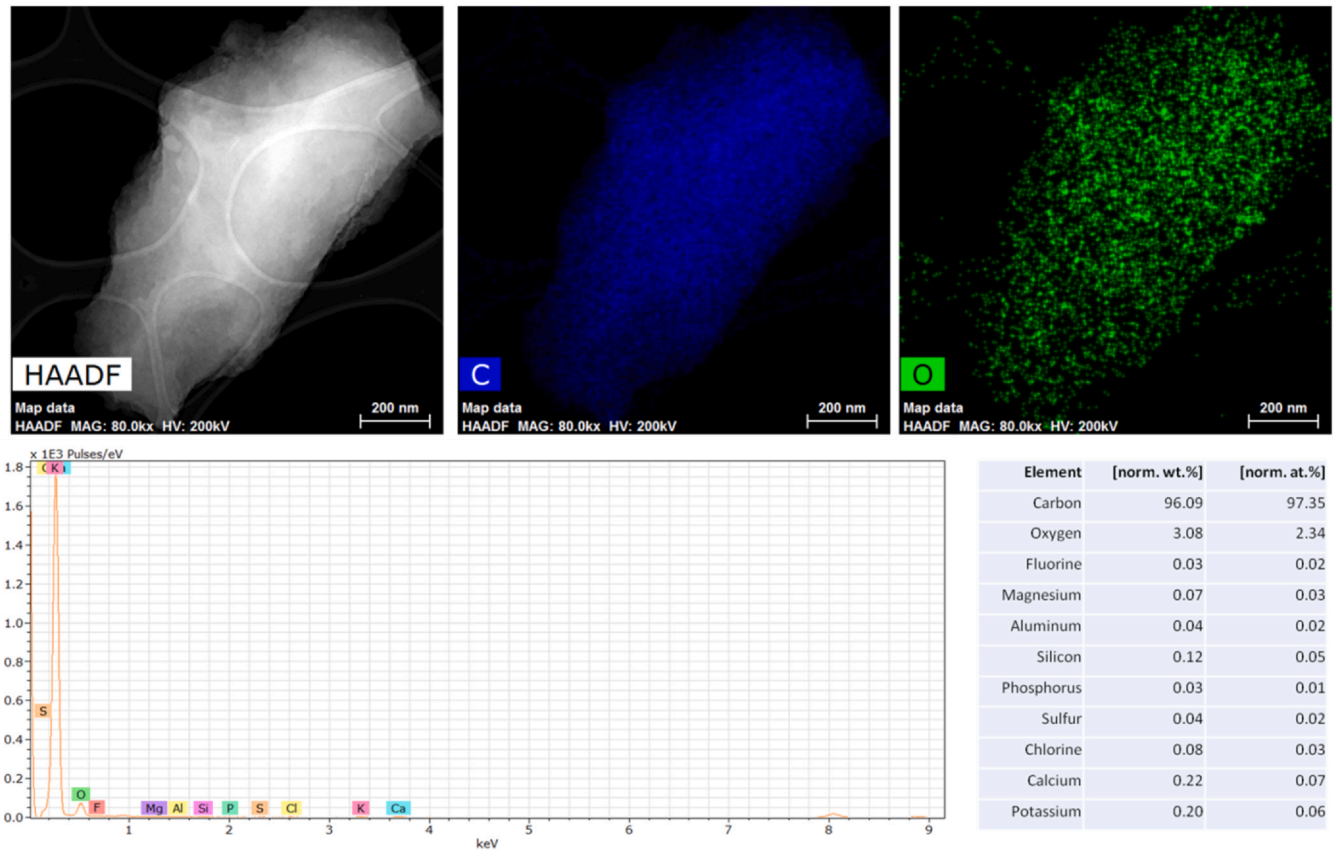

Element	[norm. wt.%]	[norm. at.%]
Carbon	96.09	97.35
Oxygen	3.08	2.34
Fluorine	0.03	0.02
Magnesium	0.07	0.03
Aluminum	0.04	0.02
Silicon	0.12	0.05
Phosphorus	0.03	0.01
Sulfur	0.04	0.02
Chlorine	0.08	0.03
Calcium	0.22	0.07
Potassium	0.20	0.06

Fig. 4. EDS analysis of AC before doping. HAADF is high-angle annular dark-field image.

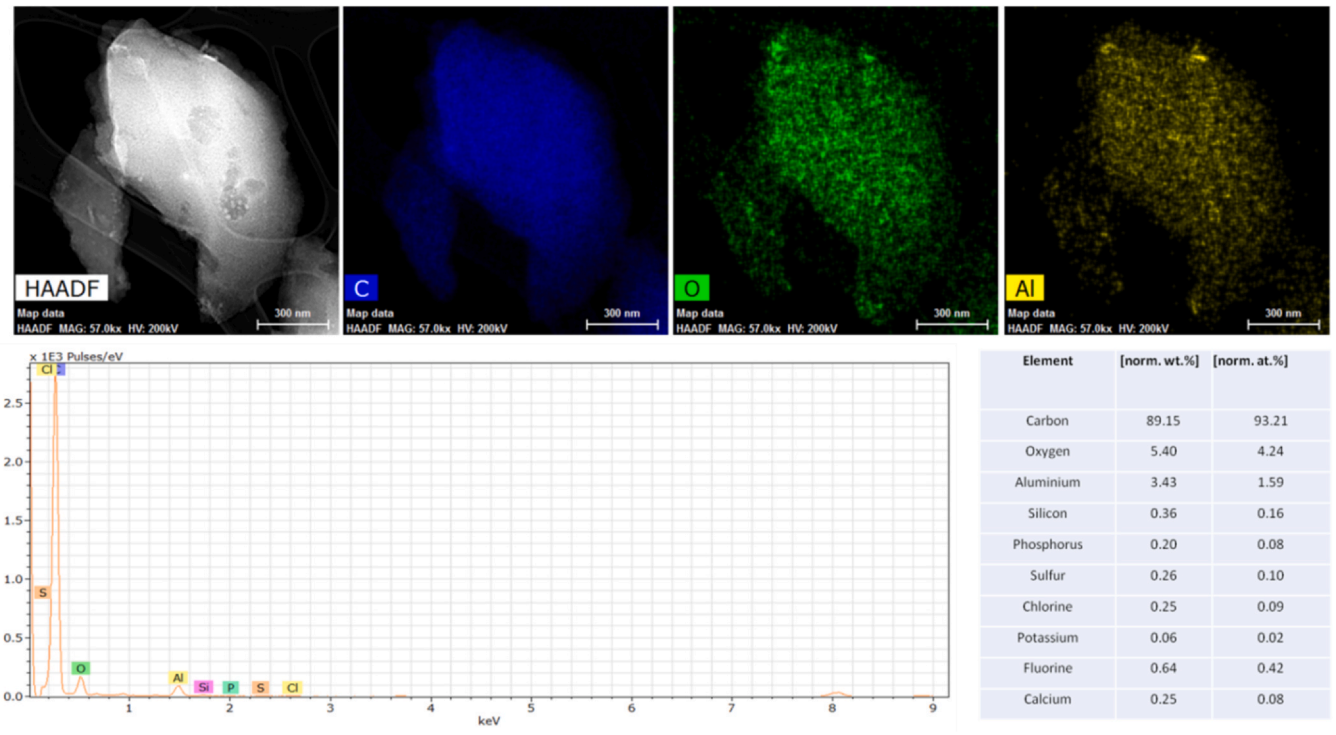

Element	[norm. wt.%]	[norm. at.%]
Carbon	89.15	93.21
Oxygen	5.40	4.24
Aluminium	3.43	1.59
Silicon	0.36	0.16
Phosphorus	0.20	0.08
Sulfur	0.26	0.10
Chlorine	0.25	0.09
Potassium	0.06	0.02
Fluorine	0.64	0.42
Calcium	0.25	0.08

Fig. 5. EDS analysis of AC doped with Al_2O_3. HAADF is high-angle annular dark-field image.

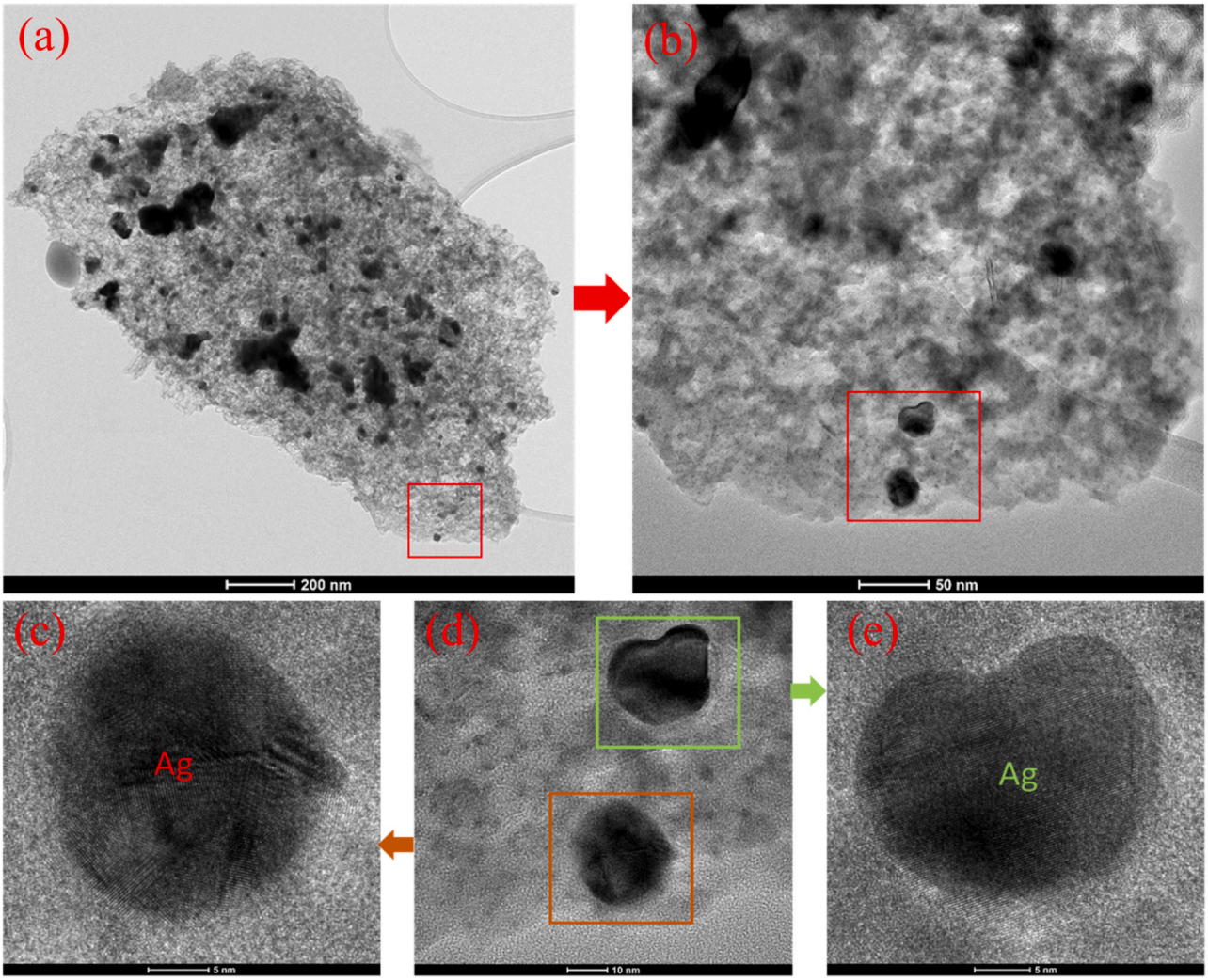

Fig. 6. TEM images of AC doped with Al_2O_3 and Ag.

ions were removed using AC, while AC-Al_2O_3 removed more than 90% of As and a negligible amount of Mo.

The removal efficiency of a contaminant on an adsorbent is a direct consequence of several factors, which include the surface charge of the adsorbent and the speciation of the adsorbate in water. The point of zero charge (PZC) of our AC was found to lie at pH 2.7, which is in agreement with the value exhibited for AC in other studies [46,47]. Therefore, AC is typically expected to carry a positive charge for pH values less than the PZC, and a negative surface charge above that value. Aluminum oxide has a PZC of approximately 9.1, hence, it carries a positive surface charge over a wide pH range [48]. Modifying AC with Al_2O_3 is expected to increase its PZC. As shown in Fig. 10, the PZC of our prepared AC-Al_2O_3 was approximately at a pH value 6.6 which indicates the successful modification of AC with Al_2O_3 nanoparticles by making it more positively charged over a broader pH range.

In order to further investigate why Mo was not adsorbed on either adsorbent in the multi-element solution and why most of the As was removed using AC-Al_2O_3, pH experiments were conducted. The effect of pH on the removal efficiency of Mo and As was conducted and the results are shown in Fig. 11a and b. The maximum percent removal for Mo was found to be at a pH 2 (97%) and decreased significantly with increasing alkalinity, reaching negligible removal at a pH 8 (Fig. 11a). A similar trend is observed by several other researchers [49–51]. It is evident that Mo adsorption on AC-Al_2O_3 was highly pH dependent. Below pH 4.5, the species of Mo that are dominant in the solution are $HMoO^{4-}$, $Mo_7O_{22}(OH)_2^{4-}$, $Mo_7O_{23}(OH)^{5-}$ and $Mo_7O_{24}^{6-}$ [51,52]. At a pH above 4.5, the MoO_4^{2-} species dominates [51]. Accordingly to Fig. 10, AC-Al_2O_3 holds a positive surface charge up to a pH 6.6 and a negative surface charge in solutions of a higher pH. The negligible removal of Mo at pH 8 suggests that Mo adsorption on AC-Al_2O_3 is dominated by an electrostatic attraction mechanism. The negatively charged Mo species were repulsed by the negatively charged AC-Al_2O_3 surface at that pH and may have also competed with OH^- ions [49].

In the case of As, in Fig. 11b, it can be seen that As was nearly completely adsorbed at the pH range of 2–4 and decreased gradually as the pH increased, reaching 94% and 78% removal at a pH 6 and pH 8, respectively. It should be mentioned at a pH < 6.8, the aqueous speciation of arsenate exists predominantly as H_2AsO^{4-}, while the divalent $HAsO_4^{2-}$ species dominates at higher pH [53]. It is hypothesized that As was removed via electrostatic attraction at the pH < pH_{PZC} between the negatively charged As species and positively charged adsorbent surface. This explains why adsorption of As at pH < pH_{pzc} was highest with respect to pH. At this pH range, the equilibrium pH was observed to increase slightly, indicating that As adsorption likely occurred as well via ion exchange between the As and hydroxide groups on the surface of the AC-Al_2O_3 adsorbent [54–57].

Since AC-Al_2O_3 held a negative charge at pH 8 and adsorption of As was still observed in Fig. 11b, adsorption by electrostatic attraction may be ruled out as the dominating adsorption mechanism for

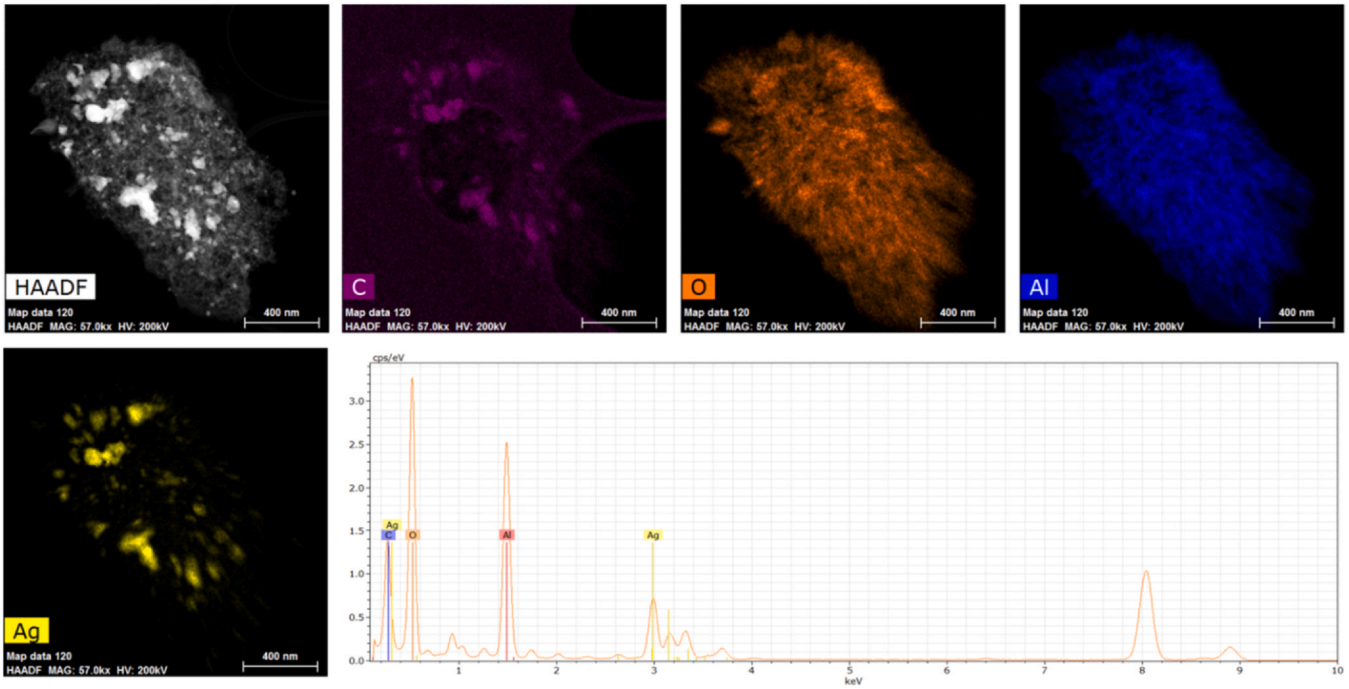

Fig. 7. EDS analysis of AC doped with Al_2O_3 and Ag. HAADF is high-angle annular dark-field image.

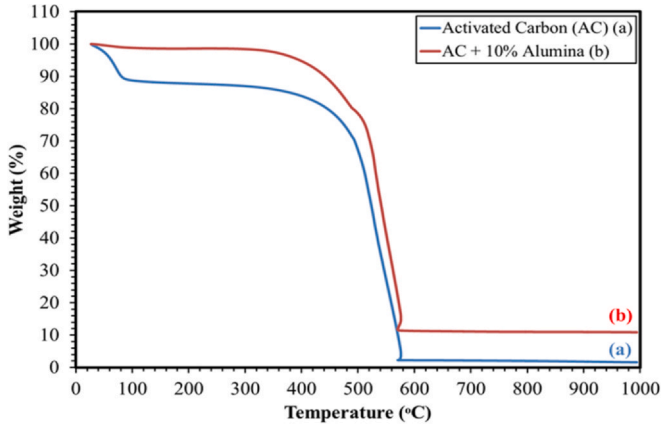

Fig. 8. TGA analysis of AC before treatment (a) and AC doped with 10 wt% Al_2O_3 (b).

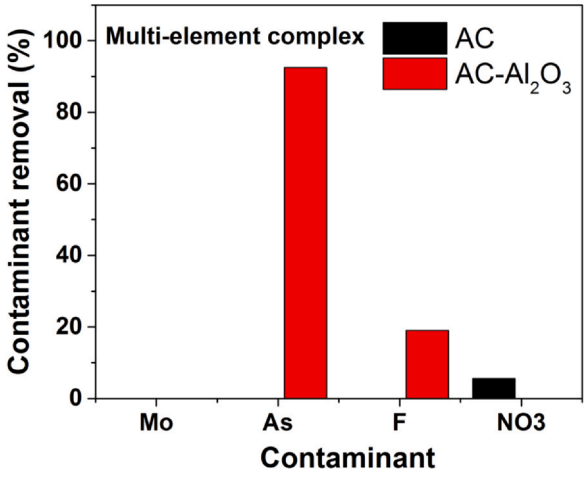

Fig. 9. As and Mo adsorption in multi-element solution (contact time = 24 h; adsorbent dosage; 2.5 g/L; pH = 7; Mo (1 mg/L), As (1 mg/L), F (5 mg/L), NO_3 (20 mg/L)) using AC and AC-Al_2O_3.

As at pH > pH_{PZC}. The results from the pH studies show that the AC-Al_2O_3 adsorbent was capable of adsorbing the negatively charged As even when it possessed a negative surface charge. This is a depiction of specific adsorption (ligand exchange or chemisorption) where a strong covalent bond forms due to the bonding of the As ion directly to the surface without the presence of a water molecule in between [58,59]. It is known that the modification of a carbon surface with oxygen-containing functional groups strongly influences its adsorption affinity towards an adsorbate [60]. The presence of oxygen in Al_2O_3 on the surface of AC leads to the formation of As–O bonds on the As/AC-Al_2O_3 interface [61]. The strong role the presence of the oxygen groups (from Al_2O_3) plays in the adsorption of As on AC confirms why AC was not capable of adsorbing As while AC-Al_2O_3 did in Fig. 9.

Leaching of Al during the As adsorption process on AC-Al_2O_3 adsorbent was tested at pH 2, pH 4, pH 6 and pH 8. Results showed Al leaching of 8.25 ± 1.52 ppm at pH 2, 0.013 ± 0.01 ppm at pH 4, 0.033 ± 0.001 ppm and 0.118 ± 0.045 at pH 6 and 8, respectively. These results show that while the material did leach in a highly acidic environment, little leaching was observed at the other pH values and the amounts lie within the US EPA secondary maximum contamination level [62].

3.3. Antibacterial properties of the prepared materials

Antibacterial properties of the synthesized materials were tested towards both Gram-negative (*E. coli*) and Gram-positive (*B. subtilis*) bacteria. Antibacterial activity by agar well diffusion technique was recorded after 24 h incubation of culture plates. Zones of inhibition of the prepared materials against the bacterial strains are displayed in Figs. 12 and 13. As seen in Fig. 12, AC and AC-Al_2O_3 materials did not show any incubation zone with tested bacteria. In contrast, zone of inhibitions for AC-Al_2O_3-Ag material against both *E.* coli and *B. subtilis* are clearly shown in Fig. 13.

The presented data indicate that AC-Al_2O_3-Ag composite material demonstrate notable antibacterial properties against the tested microorganisms. The significant zone of inhibition was exerted due to

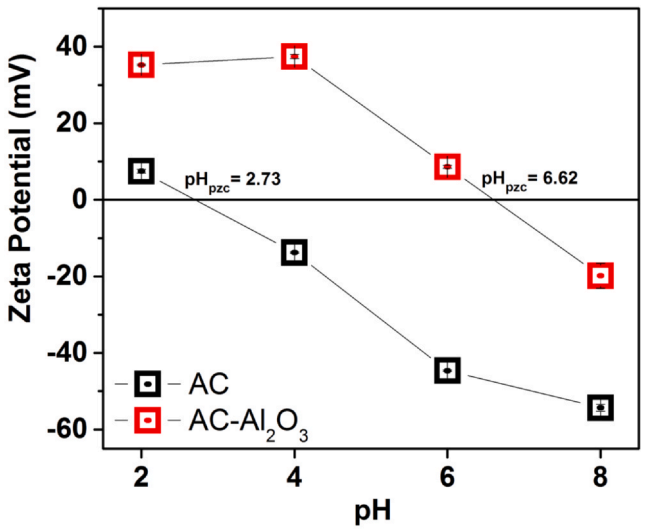

Fig. 10. Zeta potential of raw AC and AC-Al_2O_3.

bactericidal effect of doped silver on bacterial cells. Antimicrobial properties of silver-based materials have received wide attention due to the low toxicity of silver ions to human cells [63]. However, the mechanism of the bactericidal effect of silver-based materials is still not precisely identified. By using TEM, it was shown that silver nanoparticles can adhere and penetrate into *E. coli* cells and damage the cell membrane [64]. On the other hand, it was reported that Ag^+ ions released by silver-based materials interact with the respiratory chain enzymes of *E. coli* and inhibit the respiratory chain leading to cell death [65]. Marambio-Jones and Hoek [66] suggested that the most common bactericidal mechanisms of silver- based materials are as follows: (i) uptake of free silver ions followed by disruption of ATP production and DNA replication, (ii) silver particles and silver ions in the presence of dissolved oxygen generate reactive oxygen species that attack membrane lipids and lead to a breakdown of membrane and mitochondrial function or cause DNA damage, causing bacterial cell death, and (iii) silver particles directly damage to the cell membranes.

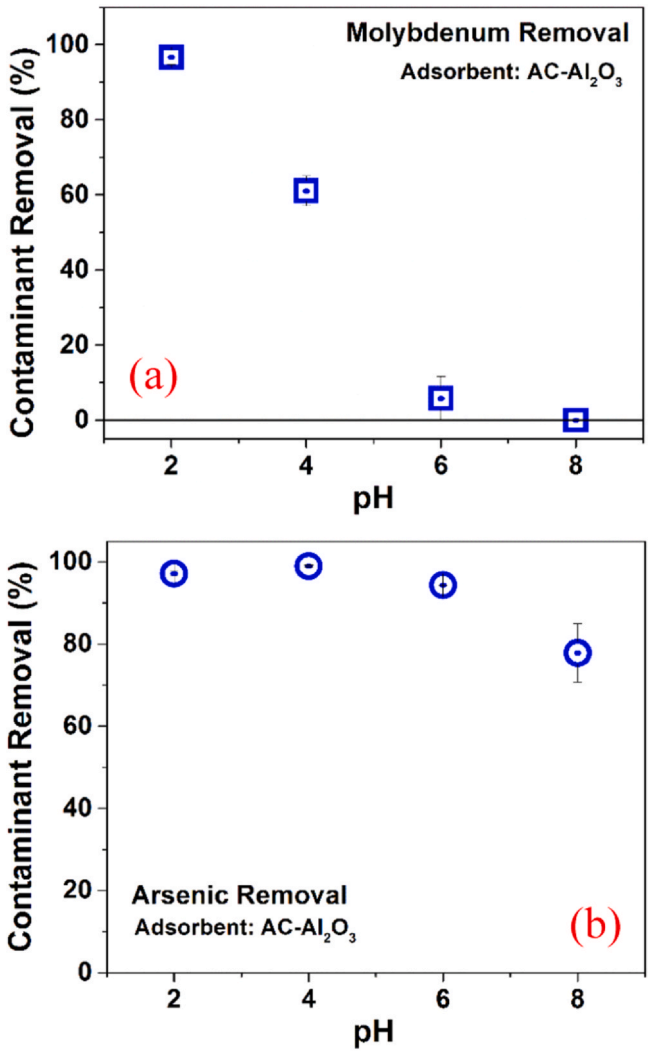

Fig. 11. Effect of pH on (a) molybdenum and (b) arsenic adsorption on AC-Al_2O_3.

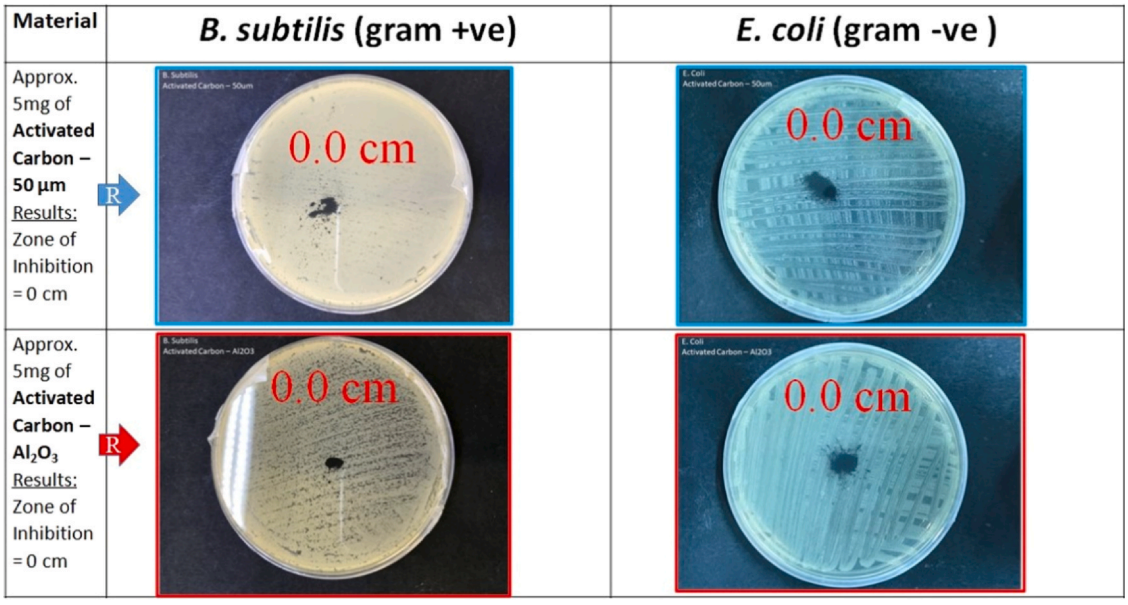

Fig. 12. Antibacterial properties of AC and AC doped 10 wt% Al_2O_3 towards gram-negative (*E. coli*) and gram-positive (*B. subtilis*) bacteria.

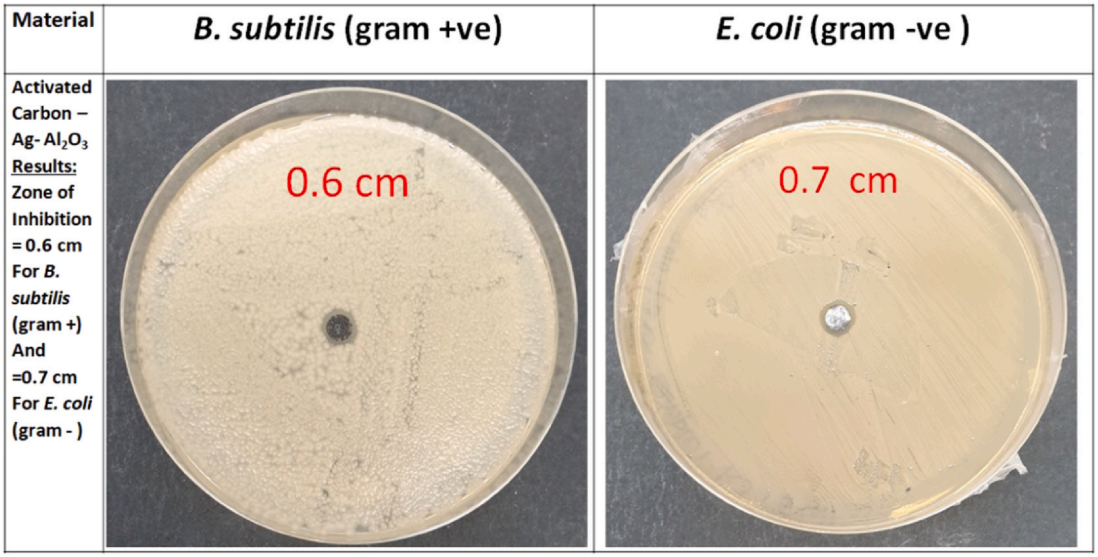

Fig. 13. Antibacterial properties of AC doped with 10 wt% Al_2O_3 and 5 wt% Ag towards gram-negative (*E. coli*) and gram-positive (*B. subtilis*).

4. Conclusions

In this study, a novel one-step thermal decomposition method was developed to prepare composite materials including AC doped with Al_2O_3 and AC doped with Al_2O_3 and Ag nanoparticles. To the best of our knowledge, this preparative method is unique, and yielded materials with promising adsorptive properties. The morphology, particle size, chemical composition, and thermal stability of the prepared composite materials were investigated by using TEM, SEM, EDS, and TGA characterization techniques.

The developed AC-Al_2O_3 materials were tested for adsorptive removal of As and Mo from multicomponent solutions in the presence of coexisting fluoride and nitrate ions, which are commonly found in natural waters. The effect of solution pH on removal efficiency was studied in detail. It was found that adsorption of Mo and As on AC-Al_2O_3 was highly pH dependent and likely involved an electrostatic attraction mechanism. The maximum Mo removal was found to be at a pH 2 (97%) and removal decreased notably with increasing feed pH value. On the other hand, As was nearly completely adsorbed at the pH range of 2–4 and the removal efficiency decreased to 94% and 78% at feed pH 6 and 8, respectively. The high adsorption of As on AC-Al_2O_3 was postulated to be based on a ligand exchange mechanism. Antibacterial properties of the developed materials were tested towards both Gram-negative (*E. coli*) and Gram-positive (*B. subtilis*) bacteria by using the agar well diffusion technique. A significant zone of inhibition was found for AC-Al_2O_3-Ag sample, indicating notable antibacterial properties of the synthesized composite material against the tested microorganisms. The high adsorptive removal of Mo and As, as well as bactericidal properties of the prepared composite materials, are promising for their application in water treatment.

CRediT authorship contribution statement

Rashad Al-Gaashani is the first and corresponding author. He conducted the material preparation and characterization in the lab. **Dema Almasri** performed the batch adsorption experiments and wrote the section. **Basem Shomar** supervised the work and revised the manuscript. **Viktor Kochkodan** is leading the research project and designed the testing of the antimicrobial properties of the synthesized material and wrote the sections. All authors revised and improved the manuscript.

Declaration of Competing Interest

The authors declare that they have no known competing financial interests or personal relationships that could have appeared to influence the work reported in this paper.

Acknowledgments

The authors would like to acknowledge the support of Qatar Environmental and Energy Research Institute and Hamad Bin Khalifa University. The authors would also like to thank the director of QEERI's Core Labs Dr. Said Mansour as well as the following Core Labs members: Omar El Hassan (TGA), Dr. Akshath Raghu Shetty (XRD), Mr. Janarthanan Ponraj (TEM) and Mr. Mujaheed Pasha (SEM) for their characterization support. The authors would also like to thank Dr. Khaled Mahmoud, Dr. Kashif Rasool and Ms Khadija for their antibacterial studies. The authors gratefully acknowledge Qatar National Library for its support. Open access funding provided by the Qatar National Library.

References

[1] A. Bhatnagar, W. Hogland, M. Marques, M. Sillanpää, An overview of the modification methods of activated carbon for its water treatment applications, Chem. Eng. J. 219 (2013) 499–511.
[2] S. Wong, N. Ngadi, I.M. Inuwa, O. Hassan, Recent advances in applications of activated carbon from biowaste for wastewater treatment: a short review, J. Clean. Prod. 175 (2018) 361–375.
[3] P. Derakhshi, H. Ghafourian, M. Khosravi, M. Rabani, Optimization of molybdenum adsorption from aqueous solution using granular activated carbon, World Appl. Sci. J. 7 (2009) 230–238.
[4] C. Nieto-Delgado, J.R. Rangel-Mendez, Anchorage of iron hydro (oxide) nanoparticles onto activated carbon to remove As (V) from water, Water Res. 46 (2012) 2973–2982.
[5] F. Haghighat, C.-S. Lee, B. Pant, G. Bolourani, N. Lakdawala, A. Bastani, Evaluation of various activated carbons for air cleaning–towards design of immune and sustainable buildings, Atmos. Environ. 42 (2008) 8176–8184.
[6] D.V. Lam, K. Jo, C.-H. Kim, J.-H. Kim, H.-J. Lee, S.-M. Lee, Activated carbon textile via chemistry of metal extraction for supercapacitors, ACS Nano 10 (2016) 11351–11359.
[7] A.Y. Tsivadze, V. Gur'yanov, G. Petukhova, Preparation of spherical activated carbon from furfural, its properties and prospective applications in medicine and the national economy, Prot. Met. Phys. Chem. Surf. 47 (2011) 612–620.
[8] A. Venault, D. Bouyer, C. Pochat-Bohatier, C. Faur, L. Vachoud, Modeling the mass transfers during the elaboration of chitosan-activated carbon composites for medical applications, AIChE J. 56 (2010) 1593–1609.
[9] M. Santiago, F. Stüber, A. Fortuny, A. Fabregat, J. Font, Modified activated carbons for catalytic wet air oxidation of phenol, Carbon 43 (2005) 2134–2145.
[10] H. Dong, H. Yu, X. Wang, Q. Zhou, J. Feng, A novel structure of scalable air-cathode without Nafion and Pt by rolling activated carbon and PTFE as catalyst layer in microbial fuel cells, Water Res. 46 (2012) 5777–5787.

[11] F. Lücking, H. Köser, M. Jank, A. Ritter, Iron powder, graphite and activated carbon as catalysts for the oxidation of 4-chlorophenol with hydrogen peroxide in aqueous solution, Water Res. 32 (1998) 2607–2614.
[12] I. Safarik, K. Horska, K. Pospiskova, M. Safarikova, Magnetically responsive activated carbons for bio- and environmental applications, Int. Rev. Chem. Eng. 4 (2012) 346–352.
[13] T.Q. Tuan, N. Van Son, H.T.K. Dung, N.H. Luong, B.T. Thuy, N.T. Van Anh, N.D. Hoa, N.H. Hai, Preparation and properties of silver nanoparticles loaded in activated carbon for biological and environmental applications, J. Hazard. Mater. 192 (2011) 1321–1329.
[14] E. Elanthamilan, S. Rajkumar, J. Princy Merlin, D. Sangeeth Jona, K. Monisha, B. Catherin Meena, Effect of decorating cobalt ferrite spinel structures on *pistachio vera* shell-derived activated carbon on energy storage applications, Electrochim. Acta 359 (2020) 136953.
[15] K. Januszewicz, A. Cymann-Sachajdak, P. Kazimierski, M. Klein, J. Łuczak, M. Wilamowska-Zawłocka, Chestnut-derived activated carbon as a prospective material for energy storage, Materials 13 (20) (2020) 4658.
[16] P. Dwivedi, V. Gaur, A. Sharma, N. Verma, Comparative study of removal of volatile organic compounds by cryogenic condensation and adsorption by activated carbon fiber, Sep. Purif. Technol. 39 (2004) 23–37.
[17] M.W. LeChevallier, T.S. Hassenauer, A.K. Camper, G.A. McFeters, Disinfection of bacteria attached to granular activated carbon, Appl. Environ. Microbiol. 48 (1984) 918–923.
[18] A.K. Camper, M.W. LeChevallier, S.C. Broadaway, G.A. McFeters, Bacteria associated with granular activated carbon particles in drinking water, Appl. Environ. Microbiol. 52 (1986) 434–438.
[19] C. Bouki, D. Venieri, E. Diamadopoulos, Detection and fate of antibiotic resistant bacteria in wastewater treatment plants: a review, Ecotoxicol. Environ. Saf. 91 (2013) 1–9.
[20] G. Gagnon, J. Rand, K. O'leary, A. Rygel, C. Chauret, R. Andrews, Disinfectant efficacy of chlorite and chlorine dioxide in drinking water biofilms, Water Res. 39 (2005) 1809–1817.
[21] P. Sommer, C. Martin-Rouas, E. Mettler, Influence of the adherent population level on biofilm population, structure and resistance to chlorination, Food Microbiol. 16 (1999) 503–515.
[22] B. Deng, M. Caviness, Z. Gu, Arsenic Removal by Activated Carbon-Based Materials, ACS Publications, 2005.
[23] W. Chen, R. Parette, J. Zou, F.S. Cannon, B.A. Dempsey, Arsenic removal by iron-modified activated carbon, Water Res. 41 (2007) 1851–1858.
[24] M.B. Baskan, A. Pala, A statistical experiment design approach for arsenic removal by coagulation process using aluminum sulfate, Desalination 254 (2010) 42–48.
[25] M.F. Ahmed, An overview of arsenic removal technologies in Bangladesh and India, in: Proceedings of the BUET-UNU International Workshop on Technologies for Arsenic Removal from Drinking Water, Dhaka, 2001, pp. 5–7.
[26] Y. Jeong, M. Fan, S. Singh, C.-L. Chuang, B. Saha, J.H. Van Leeuwen, Evaluation of iron oxide and aluminum oxide as potential arsenic (V) adsorbents, Chem. Eng. Process. Process Intensif. 46 (2007) 1030–1039.
[27] M. Habuda-Stanić, M. Nujić, Arsenic removal by nanoparticles: a review, Environ. Sci. Pollut. Res. 22 (2015) 8094–8123.
[28] T. Pichler, S. Koopmann, Should monitoring of molybdenum (Mo) in groundwater, drinking water and well permitting made mandatory? Environ. Sci. Technol. 54 (2020) 1–2.
[29] M.K. Mondal, R. Garg, A comprehensive review on removal of arsenic using activated carbon prepared from easily available waste materials, Environ. Sci. Pollut. Res. 24 (2017) 13295–13306.
[30] G.P. Gallios, A.K. Tolkou, I.A. Katsoyiannis, K. Stefusova, M. Vaclavikova, E.A. Deliyanni, Adsorption of arsenate by nano scaled activated carbon modified by iron and manganese oxides, Sustainability 9 (2017) 1684.
[31] C. Chuang, M. Fan, M. Xu, R. Brown, S. Sung, B. Saha, C. Huang, Adsorption of arsenic (V) by activated carbon prepared from oat hulls, Chemosphere 61 (2005) 478–483.
[32] F. Pagnanelli, F. Ferella, I. De Michelis, F. Vegliò, Adsorption onto activated carbon for molybdenum recovery from leach liquors of exhausted hydrotreating catalysts, Hydrometallurgy 110 (2011) 67–72.
[33] V.P. Parvathi, M. Umadevi, R. Sasikala, R. Parimaladevi, V. Ragavendran, J. Mayandi, G. Sathe, Novel silver nanoparticles/activated carbon co-doped titania nanoparticles for enhanced antibacterial activity, Mater. Lett. 258 (2020) 126775.
[34] M. Sánchez-Polo, J. Rivera-Utrilla, E. Salhi, U. von Gunten, Ag-doped carbon aerogels for removing halide ions in water treatment, Water Res. 41 (2007) 1031–1037.
[35] P. Biswas, R. Bandyopadhyaya, Water disinfection using silver nanoparticle impregnated activated carbon: Escherichia coli cell-killing in batch and continuous packed column operation over a long duration, Water Res. 100 (2016) 105–115.
[36] W. Xiong, J. Tong, Z. Yang, G. Zeng, Y. Zhou, D. Wang, P. Song, R. Xu, C. Zhang, M. Cheng, Adsorption of phosphate from aqueous solution using iron-zirconium modified activated carbon nanofiber: performance and mechanism, J. Colloid Interface Sci. 493 (2017) 17–23.
[37] S.Z. Mohammadi, Z. Darijani, M.A. Karimi, Fast and efficient removal of phenol by magnetic activated carbon-cobalt nanoparticles, J. Alloy. Compd. 832 (2020) 154942.
[38] Y. Zhao, Z.-q. Wang, X. Zhao, W. Li, S.-x. Liu, Antibacterial action of silver-doped activated carbon prepared by vacuum impregnation, Appl. Surf. Sci. 266 (2013) 67–72.
[39] S. Zhang, R. Fu, D. Wu, W. Xu, Q. Ye, Z. Chen, Preparation and characterization of antibacterial silver-dispersed activated carbon aerogels, Carbon 42 (2004) 3209–3216.
[40] N. Srinivasan, P. Shankar, R. Bandyopadhyaya, Plasma treated activated carbon impregnated with silver nanoparticles for improved antibacterial effect in water disinfection, Carbon 57 (2013) 1–10.
[41] W. Wang, K. Xiao, T. He, L. Zhu, Synthesis and characterization of Ag nanoparticles decorated mesoporous sintered activated carbon with antibacterial and adsorptive properties, J. Alloy. Compd. 647 (2015) 1007–1012.
[42] L. Jin, H. Si, J. Zhang, P. Lin, Z. Hu, B. Qiu, H. Hu, Preparation of activated carbon supported Fe–Al2O3 catalyst and its application for hydrogen production by catalytic methane decomposition, Int. J. Hydrog. Energy 38 (2013) 10373–10380.
[43] H. Hammani, W. Boumya, F. Laghrib, A. Farahi, S. Lahrich, A. Aboulkas, M. El Mhammedi, Electro-catalytic effect of Al2O3 supported onto activated carbon in oxidizing phenol at graphite electrode, Mater. Today Chem. 3 (2017) 27–36.
[44] M. Li, Z. Si, X. Wu, D. Weng, F. Kang, Facile synthesis of hierarchical porous γ-Al2O3 hollow microspheres for water treatment, J. Colloid Interface Sci. 417 (2014) 369–378.
[45] C. Perez, Antibiotic assay by agar-well diffusion method, Acta Biol. Med. Exp. 15 (1990) 113–115.
[46] C. Tang, Y. Shu, R. Zhang, X. Li, J. Song, B. Li, Y. Zhang, D. Ou, Comparison of the removal and adsorption mechanisms of cadmium and lead from aqueous solution by activated carbons prepared from Typha angustifolia and Salix matsudana, RSC Adv. 7 (2017) 16092–16103.
[47] M. Niksirat, R. Sadeghi, J. Esmaili, Removal of Mn from aqueous solutions, by activated carbon obtained from tire residuals, SN Appl. Sci. 1 (2019) 782.
[48] P. Tewari, A. McLean, Temperature dependence of point of zero charge of alumina and magnetite, J. Colloid Interface Sci. 40 (1972) 267–272.
[49] J. Lian, F. Zhou, B. Chen, M. Yang, S. Wang, Z. Liu, S. Niu, Enhanced adsorption of molybdenum (VI) onto drinking water treatment residues modified by thermal treatment and acid activation, J. Clean. Prod. 244 (2020) 118719.
[50] J. Lian, Y. Huang, B. Chen, S. Wang, P. Wang, S. Niu, Z. Liu, Removal of molybdenum (VI) from aqueous solutions using nano zero-valent iron supported on biochar enhanced by cetyl-trimethyl ammonium bromide: adsorption kinetic, isotherm and mechanism studies, Water Sci. Technol. 2018 (2017) 859–868.
[51] C. Namasivayam, D. Sangeetha, Removal of molybdate from water by adsorption onto $ZnCl_2$ activated coir pith carbon, Bioresour. Technol. 97 (2006) 1194–1200.
[52] B. Verbinnen, C. Block, D. Hannes, P. Lievens, M. Vaclavikova, K. Stefusova, G. Gallios, C. Vandecasteele, Removal of molybdate anions from water by adsorption on zeolite-supported magnetite, Water Environ. Res. 84 (2012) 753–760.
[53] W. Shao, X. Li, Q. Cao, F. Luo, J. Li, Y. Du, Adsorption of arsenate and arsenite anions from aqueous medium by using metal (III)-loaded amberlite resins, Hydrometallurgy 91 (2008) 138–143.
[54] A. Ioannou, A. Dimirkou, Phosphate adsorption on hematite, kaolinite, and kaolinite–hematite (k–h) systems as described by a constant capacitance model, J. Colloid Interface Sci. 192 (1997) 119–128.
[55] R.M. Cornell, U. Schwertmann, The Iron Oxides: Structure, Properties, Reactions, Occurrences and Uses, John Wiley & Sons, 2003.
[56] N.K. Van Alfen, Encyclopedia of Agriculture and Food Systems, Elsevier, 2014.
[57] M. Li, J. Liu, Y. Xu, G. Qian, Phosphate adsorption on metal oxides and metal hydroxides: a comparative review, Environ. Rev. 24 (2016) 319–332.
[58] S. Yao, Z. Liu, Z. Shi, Arsenic removal from aqueous solutions by adsorption onto iron oxide/activated carbon magnetic composite, J. Environ. Health Sci. Eng. 12 (2014) 58.
[59] S. Ye, W. Jin, Q. Huang, Y. Hu, B.R. Shah, S. Liu, Y. Li, B. Li, Fabrication and characterization of KGM-based FMBO-containing aerogels for removal of arsenite in aqueous solution, RSC Adv. 5 (2015) 41877–41886.
[60] M. Park, B.-H. Kim, S. Kim, D.-S. Han, G. Kim, K.-R. Lee, Improved binding between copper and carbon nanotubes in a composite using oxygen-containing functional groups, Carbon 49 (2011) 811–818.
[61] M. Poorsargol, Z. Razmara, M.M. Amiri, The role of hydroxyl and carboxyl functional groups in adsorption of copper by carbon nanotube and hybrid graphene–carbon nanotube: insights from molecular dynamic simulation, Adsorption 26 (2020) 397–405.
[62] USEPA, Secondary Drinking Water Standards: Guidance for Nuisance Chemicals, 2020.
[63] D. Williams, The biocompatibility of silver, in: Proceedings of the first International Conference on Gold and Silver in Medicine, 1987, pp. 261–272.
[64] O. Choi, K.K. Deng, N.-J. Kim, L. Ross Jr., R.Y. Surampalli, Z. Hu, The inhibitory effects of silver nanoparticles, silver ions, and silver chloride colloids on microbial growth, Water Res. 42 (2008) 3066–3074.
[65] M. Rai, A. Yadav, A. Gade, Silver nanoparticles as a new generation of antimicrobials, Biotechnol. Adv. 27 (2009) 76–83.
[66] C. Marambio-Jones, E.M. Hoek, A review of the antibacterial effects of silver nanomaterials and potential implications for human health and the environment, J. Nanopart. Res. 12 (2010) 1531–1551.